A light-sensing knot revealed by the structure of the chromophore-binding domain of phytochrome

Article *in* Nature · December 2005

DOI: 10.1038/nature04118 · Source: PubMed

4 authors, including:

Joseph S Brunzelle
Northwestern University
95 PUBLICATIONS **3,458** CITATIONS

SEE PROFILE

Katrina T Forest
University of Wisconsin–Madison
102 PUBLICATIONS **4,077** CITATIONS

SEE PROFILE

ARTICLES

A light-sensing knot revealed by the structure of the chromophore-binding domain of phytochrome

Jeremiah R. Wagner[1], Joseph S. Brunzelle[3], Katrina T. Forest[2] & Richard D. Vierstra[1]

Phytochromes are red/far-red light photoreceptors that direct photosensory responses across the bacterial, fungal and plant kingdoms. These include photosynthetic potential and pigmentation in bacteria as well as chloroplast development and photomorphogenesis in plants. Phytochromes consist of an amino-terminal region that covalently binds a single bilin chromophore, followed by a carboxy-terminal dimerization domain that often transmits the light signal through a histidine kinase relay. Here we describe the three-dimensional structure of the chromophore-binding domain of *Deinococcus radiodurans* phytochrome assembled with its chromophore biliverdin in the Pr ground state. Our model, refined to 2.5 Å resolution, reaffirms Cys 24 as the chromophore attachment site, locates key amino acids that form a solvent-shielded bilin-binding pocket, and reveals an unusually formed deep trefoil knot that stabilizes this region. The structure provides the first three-dimensional glimpse into the photochromic behaviour of these photoreceptors and helps to explain the evolution of higher plant phytochromes from prokaryotic precursors.

Prokaryotes and eukaryotes employ a complex array of photoreceptors to coordinate their response to the ambient light environment. One of the most influential is the phytochrome superfamily, a large and diverse group of photoreceptors that use a bilin (or linear tetrapyrrole) chromophore for light detection[1,2]. These photoreceptors bind bilins via a thioether linkage to a cysteine within the polypeptide, using an intrinsic lyase activity. After assembly, phytochromes sense red and far-red light through two relatively stable conformers, a red-light-absorbing Pr form and a far-red-light-absorbing Pfr form. By photoconverting between active and inactive forms, phytochromes act as light-regulated master switches in numerous signalling cascades. Phytochrome photoreceptors were first discovered in higher plants because of their ability to initiate red/far-red photoresponses of agricultural significance such as seed germination and flowering (reviewed in ref. 3). More recently, they have been found in cyanobacteria, proteobacteria, actinobacteria, fungi and slime moulds[1,4]. Despite their importance, we still do not fully understand the initial molecular events that allow phytochromes to switch reversibly between the Pr and Pfr forms, nor how this transition is transduced to appropriate sensory cascades. In an attempt to define how phytochromes work at the atomic level, we have solved the three-dimensional structure of the light-sensing region of a phytochrome from the bacterium *Deinococcus radiodurans* complexed with its native chromophore, biliverdin.

Structure determination and overall fold

The first 321 residues of *D. radiodurans* bacteriophytochrome photoreceptor (*Dr*BphP) constitute the chromophore-binding domain (*Dr*CBD) and provide a stable, soluble and spectrally active fragment of phytochrome that is amenable to structural studies (Supplementary Fig. 1)[4,5]. Although *Dr*CBD readily assembles with biliverdin to generate a protein with a normal Pr spectrum[4], its Pfr spectrum is substantially bleached, in accord with the need of a downstream PHY domain to stabilize the Pfr conformer[4,6,7]. The crystal structure of *Dr*CBD was determined by two-wavelength anomalous dispersion methods, as described in Supplementary Table 1 and the Methods.

As predicted by PFAM[8] and sequence alignments[1,4,6], two well-known domain folds were easily identified in the *Dr*CBD structure (Fig. 1). The PAS (Per/Arndt/Sim) domain encompasses residues 38 to 128 with a five-stranded antiparallel β-sheet (β2, β1, β5, β4 and β3) flanked on one side by three α helices (α1–α3). Its concave front surface is possibly a protein–protein signalling interface, on the basis of comparisons with other PAS domains bound to protein partners[9,10]. Following the PAS domain is a GAF (cGMP phosphodiesterase/adenyl cyclase/FhlA) domain, confirmed biochemically to form most of the bilin-binding pocket[1,4,6]. This domain contains a six-stranded antiparallel β sheet (β9, β10, β11, β6, β7 and β8) sandwiched between a three-helix bundle (α4, α5, α8) and α6 and α7. As in most members of the phytochrome superfamily, the PAS domain of *Dr*CBD is preceded by an ~35-residue random-coil. Within the bacterial and fungal phytochrome clades, this extension contains the cysteine that covalently binds the A ring of the bilin chromophore[4,11].

Knotted interface

The PAS and GAF domains are connected by a 10-residue linker (residues 129–138) and limited electrostatic and hydrophobic interactions at the domain interface (for example, Asp 95 to Arg 218; Arg 100 to Asp 300 and Thr 303; Gln 53 to Thr 246; His 219Cε1 to Ala 96Cβ). The most extensive interface between the domains, however, is also the most surprising feature of the *Dr*CBD structure. A deep trefoil knot is formed as the 35 N-terminal residues upstream of the PAS domain (plus 13 residues of the T7 tag) pass through the loop between β9 and α7 (Fig. 1a, c). This loop (residues 225–257) is an insertion within the otherwise structurally conserved GAF domain. The main-chain hydrogen-bonding pattern of the knot creates a small antiparallel β-sheet-like structure in which the outer

[1]Department of Genetics, [2]Department of Bacteriology, University of Wisconsin-Madison, Madison, Wisconsin 53706 USA. [3]Life Sciences Collaborative Access Team, Northwestern University, Argonne, Illinois 60439, USA.

two mini-strands are donated by the GAF domain loop, with residues from the N-terminal region of the CBD forming the central mini-strand (Figs 1c and 2a). Partly owing to a *cis*-peptide bond at residue 235, this β2′ secondary structure forms an unusual continuation of the β-sheet from the PAS domain β2. The interface extends to the GAF domain β-sheet by using the chromophore as a stepping stone (Arg 254 from β3′ to the propionate side chain of biliverdin ring B and from the propionate side chain of biliverdin ring C to Ser 272 and Ser 274 of β10) (Fig. 2a). The knot is stabilized by a small but critical hydrophobic core (Fig. 2b). The key to this knot is Ile 35; it is positioned inside the loop and makes van der Waals contacts with side chains of Leu 41 and loop residues Val 232, Leu 234, Leu 248 and Leu 253, potentially explaining why Ile 35 is necessary for protein folding in pea Phy[12] and *Agrobacterium tumefaciens* BphP2 (ref. 4). The side chain of Gln 36 from the N-terminal polypeptide spans the base of the GAF-inserted lasso and makes hydrogen bonds to main-chain atoms of Ala 225 and Arg 254, just at the entrance and exit from the GAF domain into the lasso (Fig. 2b).

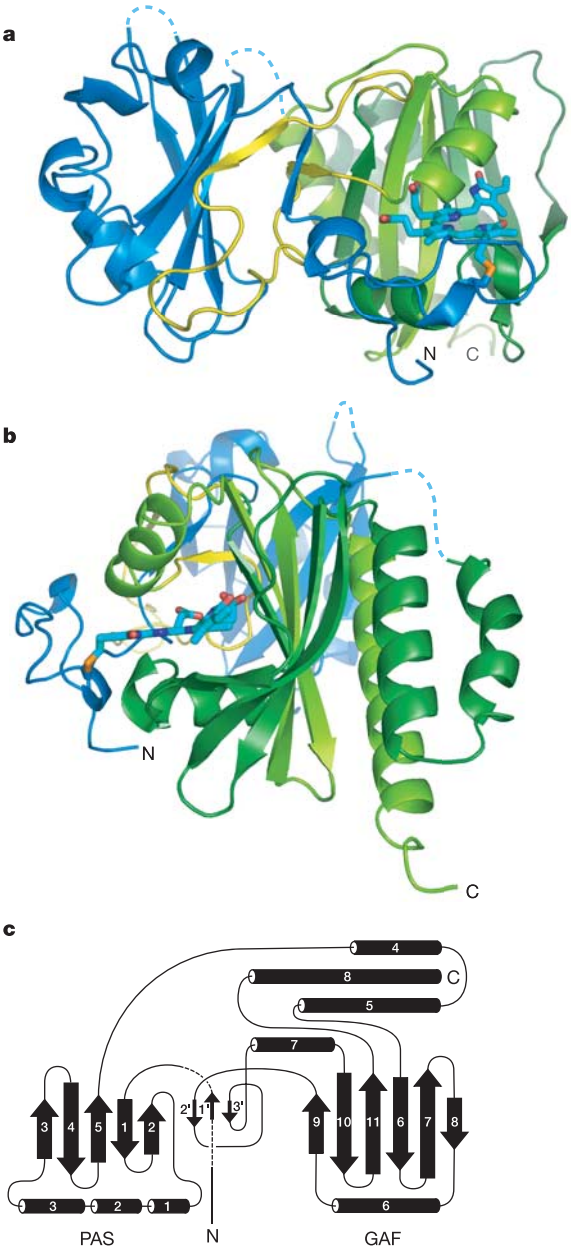

Figure 1 | Three-dimensional structure of *Dr*CBD. a, The *Dr*CBD fold consists of the N-terminal region and PAS domain (sky blue) and the GAF domain (light green for first half of sheet, yellow for lasso and dark green for second half of sheet). Biliverdin (blue) is covalently attached via thioether linkage to Cys24 (orange). Dashed lines identify disordered residues missing from the model. **b**, The nonplanar biliverdin rests in a binding groove within the GAF domain. Colours as in **a**, with model rotated ~90° about the *y* axis. **c**, Topology of CBD, including the knotted mini-sheet (centre). Numbers refer to secondary structure elements.

Although it was once considered impossible, several proteins have been identified recently with overhand, or trefoil, knots in the polypeptide chain[13–17]. The *Dr*CBD contains a rare deep trefoil knot in which 48 amino acids protrude from the crossover. Given the long-held dogma that proteins do not fold into knots, we examined experimental electron density maps (Fig. 2c) and omit maps to determine whether alternative connectivities were possible; none were found. Neither do inadvertent chain tracing through symmetry mates nor domain-swapping scenarios explain the unexpected topology[18]. Φ/ψ angles, temperature factors and the real space correlation coefficient[19] throughout this region are representative of values for the entire structure. Collectively, these data give us confidence that the knot is authentic.

Bilin chromophore structure and ligation

Biliverdin within *Dr*CBD assumes a partially extended conformation with the best fit to the electron density supporting a $5Z_{syn}$,$10Z_{syn}$,$15Z_{anti}$ configuration for the methylene linkers connecting the four pyrrole rings (Fig. 3a, b). The Z_{syn} configuration between the B and C rings and the Z_{anti} configuration between the C and D rings are in agreement with several resonance Raman spectroscopy studies of the phytochromobilin (PΦB) chromophore within plant phytochromes[20–22] as well as crystal structures of the phycocyanobilin (PCB) chromophore within the photosynthetic light-harvesting complex[23,24]. However, for the A–B linkage, the $5Z_{syn}$ conformation in our structure differs from the extended $5Z_{anti}$ conformation suggested for those systems. As is the case for bilins in solution, the A, B and C rings of biliverdin are coplanar in *Dr*CBD. The D ring is rotated 44° away from this plane (Fig. 1b). This rotation, which may strain the C15 = C16 double bond, appears to be stabilized by a hydrogen bond from the D-ring carbonyl oxygen to His 290 and by hydrophobic contacts of the D-ring vinyl group with Phe 198 and Phe 203 (Fig. 3c).

Bacterial phytochromes such as *Dr*BphP bind biliverdin via a thioether linkage between a conserved cysteine upstream of the PAS domain and the A-ring C3 vinyl group[4,11]. Our structure confirms this linkage and suggests a covalent bond to the terminal $C3^2$ carbon of the vinyl group, thus forming an extended linker between the polypeptide backbone and the bilin (Fig. 3). The intrinsic bilin lyase mechanism of phytochromes has not been resolved, although the protein structure surrounding the Cys 24 binding site suggests a possible mechanism. The side-chain carboxylates of Glu 25 and Glu 27 are 4.9 and 7.2 Å, respectively, from the Cys 24 sulphur. In the apoprotein form of this Phy, either or both residues could approach and activate the thiol for subsequent nucleophilic attack at $C3^2$. The geometry of the site and the potential for electron resonance within biliverdin may favour this reaction with the $C3^2$ carbon over the $C3^1$ carbon, which is the attachment site for the more reduced bilins in plant and cyanobacterial phytochromes (Fig. 3a). The final resolution of the attachment mechanism for biliverdin will require additional biochemical experiments.

Chromophore-binding pocket

The unique photochromicity of phytochromes results from key interactions between the bilin and its binding pocket[1,6,22]. Biliverdin slides into a crevice formed between α6 and α7 on one side and the GAF β-sheet on the other, largely burying the extended bilin within the protein (Figs 1b, 3c and 4a). The PAS domain and upstream

sequence provide little direct contact except for residues immediately surrounding the ligating Cys 24.

Consistent with previous binding studies with bilin analogues in plant phytochromes[25], the propionic-acid side chains of the B and C rings are particularly important for positioning biliverdin. These side chains penetrate deeply within the cleft between α7 and β-strands 9 and 10, and are fixed by highly conserved charge interactions, direct and water-mediated hydrogen bonds, and hydrophobic interactions (Fig. 3c). In particular, the carbonyl oxygens of the B-ring propionate form salt bridges with the amines of Arg 254 and form hydrogen bonds with the hydroxyl group of Tyr 216 and main-chain nitrogen of Ser 257, whereas the C-ring propionate oxygens hydrogen-bond to His 260 and the hydroxyl groups of Ser 272 and Ser 274. A water molecule (Wat 18) forms a water-mediated bridge between the C-ring propionate and His 290. There are also van der Waals interactions between Ile 29 and the aliphatic carbons of the B-ring propionate.

Other interactions contribute to biliverdin orientation in the pocket. Asp 207, Ile 208 and Pro 209 (the DIP motif) create a kink in the polypeptide chain between β8 and α6, allowing these residues access to the chromophore (Fig. 3c). The side chain of Asp 207 forms a hydrogen bond with its own main-chain nitrogen to stabilize this proline-induced kink, and forms a bifurcated hydrogen bond to the nitrogens of the A and B rings. There are hydrophobic interactions between Ile 208 and the C ring, between Pro 209 and the C10 carbon that links the B and C rings and between Pro 209 and the B ring. His 260, which was previously shown to be critical for biliverdin conjugation to *Dr*BphP[4,5], forms hydrogen bonds with the pyrrole nitrogens of rings B and C and its planar shape helps to fill a van der Waals sandwich between these planar rings and Leu 264. Wat 12 mediates a remarkable hydrogen-bonding network from His 260Nδ1 to the pyrrole nitrogens of biliverdin rings A, B and C (Fig. 3c).

During phototransformation from Pr to Pfr, a substantial re-orientation of ring D is expected[22,26]. A notable feature in our model of *Dr*CBD is the relatively sparse packing of side chains around the D ring to allow this rotation. Hydrophobic residues Met 174, Val 186 and Leu 286 line the pocket but are not tightly packed against the D ring. The main contacts to the D ring are polar on one edge (a hydrogen bond from the ring carbonyl to His 290Nε2) and hydrophobic on the other (Tyr 176, Tyr 263, Phe 198 and Phe 203) (Fig. 3b). Although Tyr 176 is buried under the chromophore in our Pr structure, the latter three aromatic residues are partially solvent-exposed, and the phenylalanine side chains contact the D-ring vinyl group.

Insights into the Pr to Pfr photochemistry

The crystal structure of *Dr*CBD provides insight into the unique red/far-red photochromicity of phytochromes. There is general agreement, based on spectroscopic results, that phototransformation to Pfr in plant and bacterial phytochromes involves a $15Z_{anti}$ to $15E_{anti}$ isomerization of the C15 = 16 double bond (Fig. 3a)[20,22,27,28]. Space around the D ring would allow rotation relative to the other pyrrole rings during the Pr to Pfr phototransformation with minimal interference from amino acids lining the pocket and only the clash of eclipsing methyl carbons from the C and D rings of the chromophore limiting rotation angle in either direction (Fig. 3c). Pre-existing torsional strain on the Pr D ring may serve to reduce the activation energy for rotation. The C15 = C16 isomerization would dissolve the

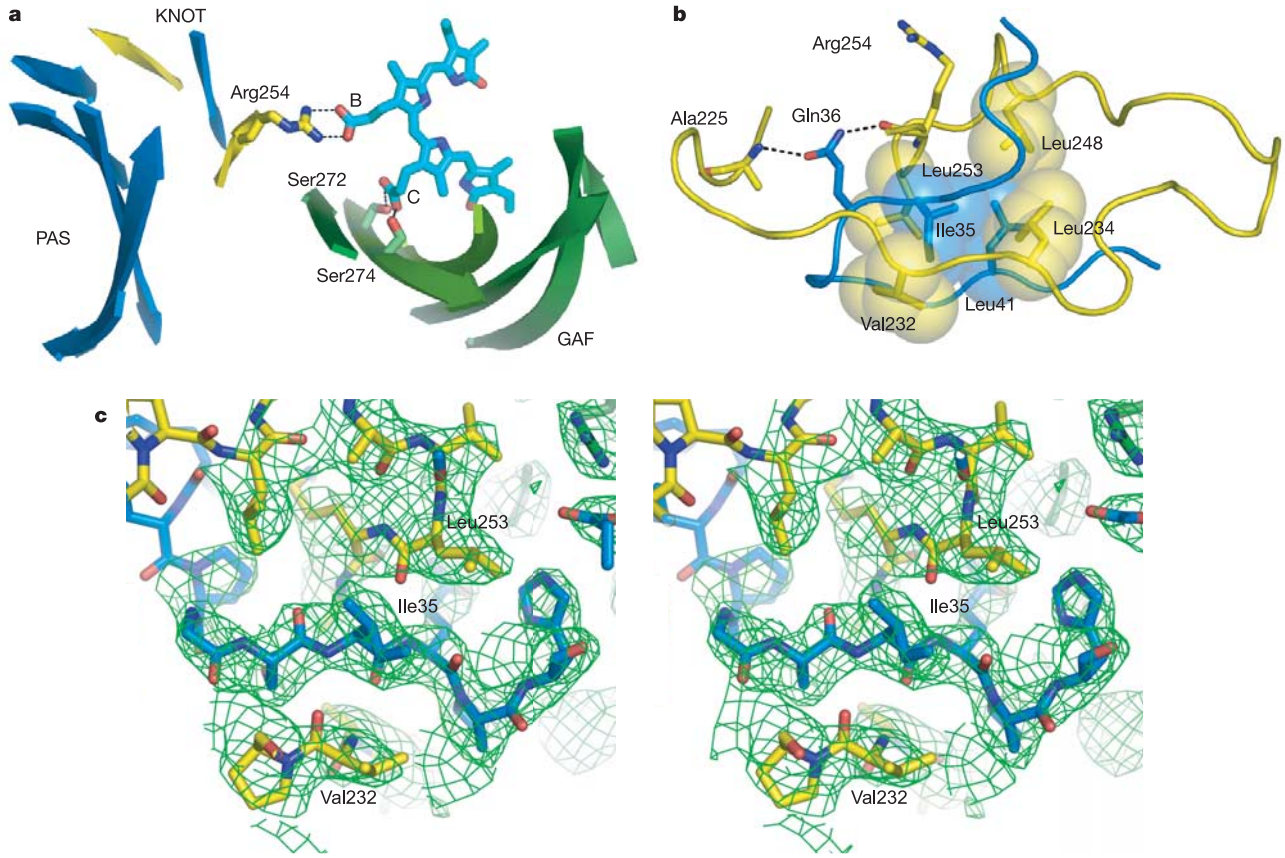

Figure 2 | Structure of the deep trefoil knot. a, A semi-continuous β-sheet 'snake' is formed by the PAS (blue) and GAF (green) domains and the polypeptide knot, with Arg 254, Ser 272 and Ser 274 stepping across the chromophore via propionate side chains of rings B and C. **b**, Conserved side chains from both the N-terminal extension (blue) and the GAF-inserted lasso (yellow) form the small hydrophobic core within the knot. **c**, Stereo depiction of the 'knot' region of the final refined model superimposed on the experimental F_o electron density map, contoured in green at 1.0σ.

interaction of the D ring with its Pr bonding partner His 290 and might perturb Phe 198 and Phe 203 by removing favourable van der Waals interactions.

In addition to rapid isomerization of the C15 = C16 bond, a subset of published experiments have predicted a torsion angle rotation from the $15E_{anti}$ to the $15E_{syn}$ configuration at the C14–C15 bond[20,22,27,28]. However, recent elegant studies with chemically locked biliverdin analogues demonstrated that the locked $15E_{anti}$ conformer of biliverdin covalently associates with a bacterial phytochrome and exhibits spectral properties similar to the Pfr form[28]. If this further $15E_{anti}$ to $15E_{syn}$ movement does occur, it would cause a steric clash between the D ring and Tyr 176 (if the rotation is away from the solvent) or Tyr 263 (if the rotation is towards the solvent). A continued rotation to the $15E_{syn}$ position could also lead to a clash with the side chain of Asp 207 (Fig. 3c).

The rotation(s) of biliverdin lead to a partial decoupling of the π conjugation system and a red-shift in the absorption spectrum of phytochrome that is characteristic of the Pfr conformer[29]. Presumably, such movement(s) induce additional conformational changes in the polypeptide to generate the distinctive shape of the Pfr conformer, which for many fungal and prokaryotic phytochromes affects the activity of an appended kinase domain[1,4]. For plant phytochromes Pfr formation exposes a nuclear localization signal in a downstream PAS-related domain[30] or uncovers interaction motifs for downstream effectors[31].

It is also possible that C15 = C16 bond isomerization could lead to perturbation of the solvent-exposed Phe side chains and that further torsion about C14–C15 could push Asp 207 and initiate local melting of the DIP motif on the surface of the CBD. Either of these would lead to a change in the shape and properties of the invariant surface patch at the chromophore-binding site (Fig. 4a). A final intriguing possibility is that even slight shifts of the orientation of B and C rings within the pocket as a consequence of D-ring movement and postulated pocket structure changes could release the propionate side chains from their electrostatic interactions. This release could break the structural bridge connecting the GAF and PAS domains and thereby free the PAS domain for signal transmission (Fig. 2a). Clearly, determining the structure of the Pfr form of CBD and of *Dr*BphP with an intact PHY domain downstream of the CBD will be essential to further understanding phototransformation and signal transduction by phytochromes, given the importance of the PHY domain to the establishment and maintenance of Pfr[4,6,7].

Functional and evolutionary implications

An important feature of the *Dr*CBD structure with respect to the rest of the phytochrome superfamily is the high degree of conservation[4,32] of essential residues that form the PAS and GAF domains, bind the bilin, and create the trefoil knot (Fig. 4a, Supplementary Fig. 2). Specific examples include the Asp-Ile-Pro (DIP) motif at the bilin-binding pocket, polar residues that interact with biliverdin propionic-acid groups (Arg 254, Ser 272 and Ser 274), bulky hydrophobic residues that line the D-ring cavity (Phe 198, Phe 203, Tyr 176 and Tyr 263), and residues that form the hydrophobic core of the trefoil knot (Ile 35, Leu 41, Leu 241 and Leu 253). For example, recent work has highlighted the importance of Tyr 176 in the photochemistry of *Synechocystis* Cph1 by showing that a His substitution at this position

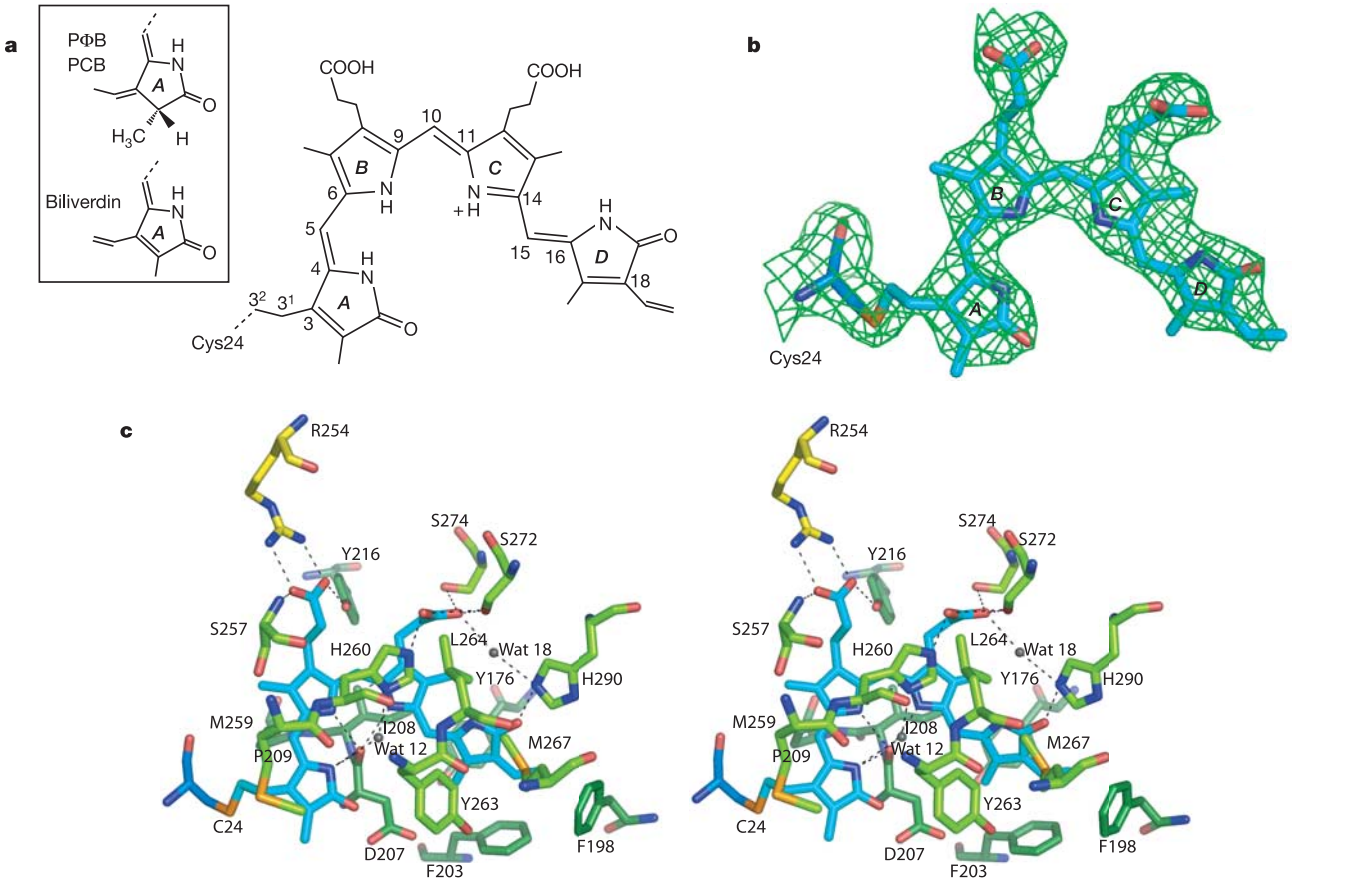

Figure 3 | Structure and linkage of biliverdin within *Dr*CBD. a, Biliverdin, attached at $C3^2$ in the A ring, adopts a $5Z_{syn}$,$10Z_{syn}$,$15Z_{anti}$ configuration. Inset, the A-ring structure for the bilin chromophore before covalent attachment to phytochrome differs for PΦB (plants) and PCB (cyanobacteria) as compared to biliverdin (bacteria). **b**, Final refined model of biliverdin is superimposed on the $2F_o - F_c$ electron density map contoured at 1.0σ. **c**, The biliverdin-binding pocket, shown here in stereo, is formed largely by invariant GAF domain residues (stick figure colour scheme as for Fig. 1a).

destabilizes Pfr and creates a red fluorophore[33]. Consequently, we expect that our structure of this bacterial phytochrome will be highly relevant to most, if not all, members of the phytochrome superfamily.

Conservation of residues surrounding the knot, including the invariant presence of the lasso loop within the GAF domain, indicates that this unique topology is common to all red/far-red photochromic phytochromes. In fact, only the loosely defined collection of bacterial phytochrome-like proteins may lack this fold, an idea based on sequence alignments that show that this group lacks both the PAS domain and the GAF loop[4]. Although several members of this phytochrome-like group bind bilins *in vitro* (RcaE, CikA and TaxD1/PixJ1)[34–36] the resulting holoproteins are not red/far-red photoreversible, suggesting that the knot is required for this spectral characteristic. Within the holoprotein, the knot may have several functions. One may be to stabilize contacts between the PAS and GAF domains. Another may be to limit the flexibility of a photoreceptor as a mechanism to prevent undesirable energy losses due to vibration or large domain movement upon photoisomerization of biliverdin. Finally, by severely restricting movement of the N-terminal domain, the knot may orient Cys 24 for efficient conjugation to biliverdin.

How do phytochromes fold into this convoluted tertiary structure? We propose a simple co-translational mechanism in which the PAS domain folds first, leaving the N-terminal 35 amino acids unstructured and Ile 35 solvent-exposed. As translation continues, the first half of the GAF domain, comprising the α4–α5 helical hairpin, the β6, β7, β8 half-sheet and α6, is translated and adopts its secondary structure. β9 is synthesized, followed by the lasso loop. The exposed hydrophobic side chains within the lasso collapse around Ile 35 to form the compact knot core. Finally, the second half of the GAF domain is translated. Although the internal symmetry of the GAF domain is interrupted by the lasso (Fig. 1a, c), the first and last β-strands cannot zip together in the centre of the sheet until translation is complete.

With respect to the evolution of this photoreceptor class, our model may explain in molecular terms how phytochromes changed from proteobacterial photoreceptors using biliverdin as the chromophore to those present today in cyanobacteria and plants that use the more reduced bilins, PCB and PΦB, respectively (Fig. 3a)[1,26]. Presumably, these blue-shifted bilins offer an adaptive advantage for sensing photosynthetic competition by closely matching the absorption spectrum of chlorophyll[3,4]. This switch required evolution of mechanisms to synthesize reduced bilins and to discriminate them from biliverdin in the lyase active site (Fig. 3a). Cyanobacterial and plant phytochromes use a cysteine in the GAF domain to bind the A-ring C3 ethylidene side chain of PCB/PΦB[37,38], as opposed to the proteobacterial and (probably) fungal phytochromes that use a cysteine upstream of the PAS domain to bind the C3 vinyl side chain of biliverdin[4,11,32]. Remarkably, modelling of this GAF cysteine into its comparable position (Met259) in *Dr*CBD reveals that it would extend towards the C3 side chain, as does Cys24 in *Dr*CBD, but from the opposite side of the chromophore (Fig. 4b). With no adjustment to the surrounding structure, the sulphur atom of a cysteine replacement at position 259 would be 5.8 Å from the Cys 24 sulphur and only 3.2 Å from the target $C3^1$ carbon of the bilin. Consequently, evolutionary transformation of the bilin attachment site could occur without structural changes, simply by acquiring a cysteine at the appropriate position in the GAF domain. In support, ref. 32 recently showed that an *Agrobacterium tumefaciens* BphP1 (Agp1) variant in which the distal cysteine was added (Val249 → Cys) preferentially assembles with PCB versus biliverdin to generate a photochromic phytochrome with typical red/far-red absorption spectra.

The structure of the bilin-binding domain of DrBphP yields the first three-dimensional insights into the photochemistry and evolution of the phytochrome superfamily. This structure provides molecular explanations for the known physico-chemical features of phytochromes, for Pr to Pfr photoconversion events that initiate responses of behavioural and agricultural significance, and for the evolution of the phytochrome family.

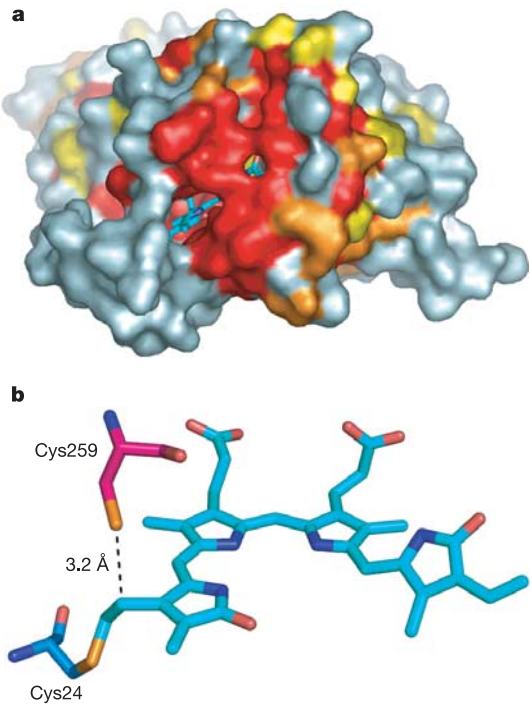

Figure 4 | Structural conservation and evolution of phytochrome photoreceptors. a, phytochrome superfamily conservation is apparent in this solvent-accessible surface of *Dr*CBD. It is colour-coded, based on 90% (red), 75% (orange) and 60% (yellow) sequence identity among phytochromes from 17 proteobacteria, 3 cyanobacteria, 3 fungi and 17 plants. (A subset of these sequences are aligned in Supplementary Fig. 2.) Invariant residues Asp 207, Tyr 263 and Phe 203 form the bridge over the deeply buried biliverdin and the two conformations observed (although not refined) in our electron density map for Tyr 263 may play a part in allowing access to the pocket. **b**, Evolution of the plant phytochrome ligand attachment site would have required the change of a single amino acid, as shown in this view of the binding site in which the *Dr*CBD Cys 24 and biliverdin (cyan) are shown with Met 259 modelled as a cysteine (Cys 259, magenta).

METHODS

Protein production and crystallization. The coding region for the first 321 (of 755 total) amino acids of *Dr*BphP (ref. 5) was amplified from a plasmid bearing the full-length gene[5,39] and introduced into pET21a(+) (Novagen) for expression with a 14-amino-acid N-terminal T7 tag and a C-terminal hexahistidine tag. A point mutation leading to a Pro 240 → Thr 240 substitution was inadvertently introduced during cloning, but the CBD bearing this mutation was photochemically identical to the CBD with the native sequence[4] (Supplementary Fig. 1). Purification, crystallization and cryoprotection were performed under green safe lights. Expression, chromophore ligation in crude lysate, and purification by Ni^{2+}-chelate affinity chromatography were carried out as described[4] with the addition of an anion-exchange (Mono-Q, Amersham) step, using a 100–500 mM NaCl elution gradient. To obtain selenomethionine-derivatized protein, *Dr*CBD apoprotein was expressed in *Escherichia coli* strain B834:pLysS (Stratagene) grown in selenomethionine expression medium (Athena Enzyme Systems/Molecular Dimensions) supplemented with 0.25 mg per litre of L-selenomethionine (Sigma)[40]. Notably, even with several methionines within the bilin-binding pocket, the binding efficiency for ligand and the action spectrum of the selenomethionine-labelled protein are indistinguishable from the native protein (Supplementary Fig. 1).

Initial crystallization conditions were identified in a 1,536-condition screen

using microbatch under oil[41] conducted by the Hauptman Woodward Institute (http://www.hwi.buffalo.edu). These conditions were optimized, and a recrystallization step was added to obtain diffraction-quality crystals. Briefly, large-scale sitting drops (75 μl of 30 mg ml^{-1} protein in 30 mM pH 8.0 Tris-HCl equilibrated with an equal volume of mother liquor, consisting of 67 mM pH 4.95 sodium acetate, 3.3% PEG 400, 1 mM DTT) yielded showers of microcrystals within 24 h at room temperature. These were harvested by centrifugation, redissolved in 30 mM pH 8.0 Tris-HCl, clarified by centrifugation, and concentrated to 20 mg ml^{-1}. Macrocrystals were grown by hanging-drop vapour diffusion using 2 μl each of protein and mother liquor; spectroscopy confirmed that crystalline *Dr*CBD is largely in the Pr state (Supplementary Fig. 1). Cryoprotection of the ~0.3 mm × 0.3 mm × 0.05 mm bright green plates in mother liquor plus 30% 2-methyl-2,4-pentanediol yielded diffraction to a maximum resolution of 2.5 Å. Native and selenomethionine-containing crystals are of the same orthorhombic space group $P2_12_12$ ($a = 64.9$ Å, $b = 133.7$ Å, $c = 49.9$ Å; $\alpha = \beta = \gamma = 90°$) with a single molecule per asymmetric unit.

Structure determination. MAD (multiwavelength anomalous dispersion) data were collected at 98 K on a MarCCD (charge-coupled device) detector at Sector 32 ID-B at the Advanced Photon Source. Inflection and peak data sets were collected on separate crystals, and integrated and merged with HKL2000[42] (Supplementary Table 1). The program Hyss[43] was used to find seven of nine possible selenium sites, five of which were refined in SHARP[44]. Initial phases, with an overall figure of merit of 0.41, were improved by solvent flattening and phase extension, and provided an interpretable electron density map. Automatic model building with ARP/wARP[45] and RESOLVE[46] placed ~40 correct amino acids and a polyalanine backbone for ~50% of the protein. The remaining model was traced manually with XFIT[47] alternated with TLS and positional refinement against the 2.5 Å inflection data set using REFMAC5[48]. Early in the refinement, electron density for biliverdin was apparent and the chromophore was fitted manually to the density. A modified amino acid in which Cys 24 was bonded to C3^2 of the A-ring vinyl group of biliverdin via a thioether linkage was refined without an energy penalty for rotation about the C15 = C16 double bond. Negative density around this bond in an electron density map calculated with Fourier coefficients F_{obs}(final 30° of data) − F_{obs}(first 30° of data) suggests that the bond is subject to radiation-induced breakage.

The final refined model includes 309 amino acid residues (residues 5–321 of *Dr*CBD and four C-terminal His residues, with two disordered residues omitted at the tip of the β3–β4 hairpin and six in the interdomain linker), biliverdin, and 34 well-ordered water molecules. Histidine residues in the purification tag form crystal-packing interactions (His 322 to the backbone of Val 318, His 325 to symmetry-related Glu 104, and His 323 to symmetry-related Glu 130). Only two non-glycine residues, Cys 24 and His 110, fall outside the favourable or most-favourable regions of the Ramachandran plot. Ligand attachment at Cys 24 may cause backbone strain, and His 110 precedes the β-hairpin break. The aromatic ring of Phe 8 was modelled in two orientations, each having occupancy of 0.5. Other sidechains showed evidence of dual conformers but were not split owing to the limited resolution of our data. The final model has very good stereochemistry, an R_{work} of 23.7%, and an R_{free} of 26.6% for all data to 2.5 Å (Supplementary Table 1).

Structure figures were generated using Pymol (Delano Scientific, San Carlos, http://pymol.sourceforge.net/).

Received 27 May; accepted 9 August 2005.

1. Vierstra, R. D. & Karniol, B. in *Handbook of Photosensory Receptors* (eds Briggs, W. R. & Spudich, J. L.) 171–196 (Wiley, Weinheim, 2005).
2. Quail, P. H. Phytochrome photosensory signalling networks. *Nature Rev. Mol. Cell Biol.* **3,** 85–93 (2002).
3. Smith, H. Physiological and ecological functions with the phytochrome family. *Annu. Rev. Plant Physiol. Plant Mol. Biol.* **46,** 269–315 (1995).
4. Karniol, B., Wagner, J. R., Walker, J. M. & Vierstra, R. D. Phylogenetic analysis of the phytochrome superfamily reveals distinct microbial subfamilies of photoreceptors. *Biochem. J.* **392,** 103–116 (2005).
5. Davis, S. J., Vener, A. V. & Vierstra, R. D. Bacteriophytochromes: phytochrome-like photoreceptors from nonphotosynthetic eubacteria. *Science* **286,** 2517–2520 (1999).
6. Wu, S. H. & Lagarias, J. C. Defining the bilin lyase domain: lessons from the extended phytochrome superfamily. *Biochemistry* **39,** 13487–13495 (2000).
7. Cherry, J. R. *et al.* Carboxy-terminal deletion analysis of oat phytochrome A reveals the presence of separate domains required for structure and biological activity. *Plant Cell* **5,** 565–575 (1993).
8. Bateman, A. *et al.* The Pfam protein families database. *Nucleic Acids Res.* **32D,** 138–141 (2004).
9. Yildiz, O. *et al.* Crystal structure and interactions of the Pas repeat region of the *Drosophila* clock protein Period. *Mol. Cell* **17,** 69–82 (2005).
10. Razeto, A. *et al.* Structure of the Ncoa-1/Src-1 Pas-B domain bound to the LxxII motif of the Stat6 transactivation domain. *J. Mol. Biol.* **336,** 319–329 (2004).
11. Lamparter, T. *et al.* The biliverdin chromophore binds covalently to a conserved cysteine residue in the N-terminus of *Agrobacterium* phytochrome Agp1. *Biochemistry* **43,** 3659–3669 (2004).
12. Bhoo, S. H. *et al.* Phytochrome photochromism probed by site-directed mutations and chromophore esterification. *J. Am. Chem. Soc.* **48,** 11717–11718 (1997).
13. Taylor, W. R. A deeply knotted protein structure and how it might fold. *Nature* **406,** 916–919 (2000).
14. Nureki, O. *et al.* An enzyme with a deep trefoil knot for the active-site architecture. *Acta Crystallogr. D* **58,** 1129–1137 (2002).
15. Taylor, W. R. & Lin, K. Protein knots: a tangled problem. *Nature* **421,** 25 (2003).
16. Zarembinski, T. I. *et al.* Deep trefoil knot implicated in RNA binding found in an archaebacterial protein. *Proteins Struct. Funct. Genet.* **50,** 177–183 (2003).
17. Mallam, A. L. & Jackson, S. E. Folding studies on a knotted protein. *J. Mol. Biol.* **346,** 1409–1421 (2005).
18. Liu, Y. & Eisenberg, D. 3D domain swapping: as domains continue to swap. *Protein Sci.* **11,** 1285–1299 (2002).
19. Vaguine, A. A., Richelle, J. & Wodak, S. J. SFCHECK: a unified set of procedures for evaluating the quality of macromolecular structure-factor data and their agreement with the atomic model. *Acta Crystallogr. D* **55,** 191–205 (1999).
20. Kneip, C. *et al.* Protonation state and structural changes of the tetrapyrrole chromophore during the Pr → Pfr phototransformation of phytochrome: a resonance Raman spectroscopic study. *Biochemistry* **38,** 15185–15192 (1999).
21. Mroginski, M. A. *et al.* Determination of the chromophore structures in the photoinduced reaction cycle of phytochrome. *J. Am. Chem. Soc.* **126,** 16734–16735 (2004).
22. Braslavsky, S. E. in *Photochromisms, Molecules and Systems* (eds BrouasLaurent, H. & BrouasLaurent, D. H.) 738–755 (Elsevier Science, Amsterdam, 2003).
23. Duerring, M., Schmidt, G. B. & Huber, R. Isolation, crystallization, crystal structure analysis and refinement of constitutive C-phycocyanin from the chromatically adapting cyanobacterium *Fremyella diplosiphon* at 1.66 Å resolution. *J. Mol. Biol.* **217,** 577–592 (1991).
24. Brejc, K., Ficner, R., Huber, R. & Steinbacher, S. Isolation, crystallization, crystal structure analysis and refinement of allophycocyanin from the cyanobacterium *Spirulina platensis* at 2.3 Å resolution. *J. Mol. Biol.* **249,** 424–440 (1995).
25. Hanzawa, H. *et al. In vitro* assembly of phytochrome B apoprotein with synthetic analogs of the phytochrome chromophore. *Proc. Natl Acad. Sci. USA* **98,** 3612–3617 (2001).
26. Tu, S.-L. & Lagarias, J. C. in *Handbook of Photosensory Receptors* (eds Briggs, W. R. & Spudich, J. L.) 121–149 (Wiley, Weinheim, 2005).
27. Fodor, S. P., Lagarias, J. C. & Mathies, R. A. Resonance Raman analysis of the Pr and Pfr forms of phytochrome. *Biochemistry* **29,** 11141–11146 (1990).
28. Inomata, K. *et al.* Sterically locked synthetic bilin derivatives and phytochrome Agp1 from *Agrobacterium tumefaciens* form photosensitive Pr- and Pfr-like adducts. *J. Biol. Chem.* **280,** 24491–24497 (2005).
29. Gartner, W. & Braslavsky, S. E. in *Photoreceptors in Light Signaling* (ed. Baschauer, A.) 136–180 (Royal Soc. Chemistry, Cambridge, UK, 2004).
30. Cheng, M., Tao, Y., Lim, J., Shaw, A. & Chory, J. Regulation of phytochrome B nuclear localization through light-dependent unmasking of nuclear-localization signals. *Curr. Biol.* **15,** 637–642 (2005).
31. Ryu, J. S. *et al.* Phytochrome-specific type 5 phosphatase controls light signal flux by enhancing phytochrome stability and affinity for a signal transducer. *Cell* **120,** 395–406 (2005).
32. Lamparter, T. *et al.* Biliverdin binds covalently to Agrobacterium phytochrome Agp1 via its ring A vinyl side chain. *J. Biol. Chem.* **278,** 33786–33792 (2003).
33. Fischer, A. J. & Lagarias, J. C. Harnessing phytochrome's glowing potential. *Proc. Natl Acad. Sci. USA* **101,** 17334–17339 (2004).
34. Mutsuda, M., Michel, K. P., Zhang, X. F., Montgomery, B. L. & Golden, S. S. Biochemical properties of CikA, an unusual phytochrome-like histidine protein kinase that resets the circadian clock in *Synechococcus elongatus* PCC 7942. *J. Biol. Chem.* **278,** 19102–19110 (2003).
35. Terauchi, K., Montgomery, B. L., Grossman, A. R., Lagarias, J. C. & Kehoe, D. M. RcaE is a complementary chromatic adaptation photoreceptor required for green and red light responsiveness. *Mol. Microbiol.* **51,** 567–577 (2004).
36. Yoshihara, S., Katayama, M., Geng, X. X. & Ikeuchi, M. Cyanobacterial phytochrome-like PixJ1 holoprotein shows novel reversible photoconversion between blue- and green-absorbing forms. *Plant Cell Physiol.* **45,** 1729–1737 (2004).
37. Lagarias, J. C. & Rapoport, H. Chromopeptides from phytochrome. The structure and linkage of the Pr form of the phytochrome chromophore. *J. Am. Chem. Soc.* **102,** 4821–4828 (1980).
38. Yeh, K. C., Wu, S. H., Murphy, J. T. & Lagarias, J. C. A cyanobacterial phyto-chrome two-component light sensory system. *Science* **277,** 1505–1508 (1997).

39. Bhoo, S. H., Davis, S. J., Walker, J., Karniol, B. & Vierstra, R. D. Bacteriophytochromes are photochromic histidine kinases using a biliverdin chromophore. *Nature* **414,** 776–779 (2001).
40. Ramakrishnan, V., Finch, J. T., Graziano, V., Lee, P. L. & Sweet, R. M. Crystal structure of globular domain of histone H5 and its implications for nucleosome binding. *Nature* **362,** 219–223 (1993).
41. Chayen, N. E., Shaw-Stewart, P. D. & Blow, D. M. Microbatch crystallization under oil—a new technique allowing many small-volume crystallization trials. *J. Cryst. Growth* **122,** 176–180 (1992).
42. Otwinowski, Z. & Minor, W. in *Macromolecular Crystallography* Part A (eds Carter, C. W. Jr & Sweet, R. M.) 307–326 (Academic, New York, 1997).
43. Grosse-Kunstleve, R. W. & Adams, P. D. Substructure search procedures for macromolecular structures. *Acta Crystallogr. D* **59,** 1974–1977 (2003).
44. Bricogne, G., Vonrhein, C., Flensburg, C., Schiltz, M. & Paciorek, W. Generation, representation and flow of phase information in structure determination: recent developments in and around SHARP 2.0. *Acta Crystallogr. D* **59,** 2023–2030 (2003).
45. Perrakis, A., Morris, R. M. & Lamzin, V. S. Automated protein model building combined with iterative structure refinement. *Nature Struct. Biol.* **6,** 458–463 (1999).
46. Terwilliger, T. SOLVE and RESOLVE: automated structure solution, density modification, and model building. *J. Synch. Radiat.* **11,** 49–52 (2004).
47. McRee, D. E. XtalView Xfit—A versatile program for manipulating atomic coordinates and electron density. *J. Struct. Biol.* **125,** 156–165 (1999).
48. Winn, M. D., Isupov, M. N. & Murshudov, G. N. Use of TLS parameters to model anisotropic displacements in macromolecular refinement. *Acta Crystallogr. D* **57,** 122–133 (2001).

Supplementary Information is linked to the online version of the paper at www.nature.com/nature.

Acknowledgements We thank B. Karniol, S. Beale and K. Satyshur for technical advice and acknowledge the Michigan Economic Development Corporation and the Michigan Technology Tri-Corridor for the support of this research program. Use of the Advanced Photon Source was supported by the US Department of Energy, Office of Science, Office of Basic Energy Sciences. This work was supported by grants from the US National Science Foundation (R.D.V. and K.T.F.), the US Department of Energy (R.D.V.), and the W.M. Keck Foundation (K.T.F.).

Author Contributions J.R.W. purified protein and grew and characterized crystals; J.S.B. collected data and carried out initial phase determination; K.T.F. and J.R.W. phased, modelled, refined and validated structure; R.D.V. initiated collaboration; K.T.F. designed structure experiments; J.R.W., K.T.F. and R.D.V. interpreted the structure and prepared the manuscript and figures.

Author Information Atomic coordinates and structure factor amplitudes have been deposited in the Protein Data Bank (accession code 1ZTU). Reprints and permissions information is available at npg.nature.com/reprintsandpermissions. The authors declare no competing financial interests. Correspondence and requests for materials should be addressed to K.T.F. (forest@bact.wisc.edu).